Editors' Suggestion

Modeling internal rogue waves in a long wave-short wave resonance framework

H. N. Chan,[1,*] R. H. J. Grimshaw,[2] and K. W. Chow[1]
[1]*Department of Mechanical Engineering, University of Hong Kong, Pokfulam, Hong Kong*
[2]*Department of Mathematics, University College London, London WC1E 6BT, United Kingdom*

(Received 13 February 2018; published 4 December 2018)

A resonance between a long wave and a short wave occurs if the phase velocity of the long wave matches the group velocity of the short wave. Rogue waves modeled as special breathers (pulsating modes) can arise from these resonant interactions. This scenario is investigated for internal waves in a density stratified fluid. We examine the properties of these rogue waves, such as the polarity, amplitude and robustness, and show that these depend critically on the specific density stratification and the choice of the participating modes. Three examples, namely, a two-layered fluid, a stratified fluid with constant buoyancy frequency, and a case of variable buoyancy frequency are examined. We show that both elevation and depression rogue waves are possible, and the maximum displacements need not be confined to a fixed ratio of the background plane wave. Furthermore, there is no constraint on the signs of nonlinearity and dispersion, nor any depth requirement on the fluid. All these features contrast sharply with those of a wave packet evolving on water of finite depth governed by the nonlinear Schrödinger equation. The amplitude of these internal rogue waves generally increases when the density variation in the layered or stratified fluid is smaller. For the case of constant buoyancy frequency, critical wave numbers give rise to nonlinear evolution dynamics for "long wave-short wave resonance," and also separate the focusing and defocusing regimes for narrow-band wave packets of the nonlinear Schrödinger equation. Numerical simulations are performed by using baseband modes as initial conditions to assess the robustness of these rogue waves in relation to the modulation instability of a background plane wave.

DOI: 10.1103/PhysRevFluids.3.124801

I. INTRODUCTION

Internal waves in the ocean constitute a rich source for fundamental scientific studies and are also of great practical importance [1]. These large amplitude displacements in the interior of the ocean can affect the distribution of nutrients, pollution, sediment transport, acoustic transmission, marine submersibles and offshore structures, important bearings on acoustic transmission, and safety of marine infrastructures. Consequently there have been extensive theoretical studies, numerical simulations, and oceanic observations. These range from the large-amplitude long waves in shallow water, often modeled by the Korteweg-de Vries equation [2,3], to the vertically propagating internal waves in the interior of the ocean which are often linked to mixing events through wave breaking [4,5].

A resonance among three linear waves arises if their frequencies (ω) and wave numbers (k) match ($\omega(k_3) = \omega(k_1) + \omega(k_2)$, $k_3 = k_1 + k_2$). A special case is "long wave-short wave" resonance

*Present address: Department of Mathematics, Chinese University of Hong Kong, Shatin, Hong Kong; hnchan@math.cuhk.edu.hk

($k_3 \approx k_1, k_2 \ll 1$), which can occur between a long internal wave and a much shorter surface wave, if the phase velocity of the long wave matches the group velocity of the short wave [6,7]. Evolution equations for the weakly nonlinear wave packet of the short wave and the long interfacial wave were derived using a two-layer fluid model using a multiple scale perturbation technique [8]. A similar set of model equations has also been derived for a continuously stratified fluid [9,10]. This long-short wave resonance occurs on a time scale of $\varepsilon^{4/3}t$, where ε is a small amplitude parameter, and is thus asymptotically faster than the $\varepsilon^2 t$ time scale of the much studied nonlinear Schrödinger equation (NLSE) [7]. The precise definition of ε in terms of properties of the fluid flows will be given in Sec. II.

There has been intense recent interest in rogue waves, which are locally and temporally confined large amplitude displacements from an equilibrium position [11]. In the ocean, such surface rogue waves clearly pose immense danger to ships and offshore structures [11,12]. Further, rogue waves can arise in other physical contexts [13]. A frequently used model for a rogue wave is the Peregrine breather of the NLSE, an exact solution algebraically localized in both space and time. The Peregrine breather has been generated and observed experimentally in water wave tanks [14]. Recently the time-reversal approach was implemented in numerical wave tanks and wave flumes to study rogue waves [15–17]. We are particularly concerned here with the sign of the main displacement of the rogue wave. As the integral of the intensity over the entire spatial domain is a constant for the NLSE, a region of depression must also accompany a rise in water level above the average position. The commonly accepted terminology in the literature is to term the Peregrine breather or similar modes as an elevation rogue wave, if the displacement of the largest amplitude is above the mean level.

In this paper we examine if rogue waves with such unexpectedly large displacements are possible also for internal waves, using the long-short wave resonance model, and examine whether both depression and elevation waves are feasible. Since energy tends to be concentrated in the oceanic waves with lower frequencies, it is especially important to study long internal rogue waves [18]. The answers to both questions are affirmative. Several theoretical studies on the system of model nonlinear evolution equations for a long-short wave resonance have been performed [19–21]. The rogue wave modes of this system can be derived by the bilinear Hirota method or the Darboux transformation. Previous studies have indicated that although the short wave packet can exhibit depression waves as well as elevation waves, the long wave component was still only an elevation wave [20]. Our main goals here are to examine this further in the internal wave context, and to demonstrate that the long wave component can experience a polarity change, that is, a conversion from a depression mode to an elevation mode, or vice versa. Such reversal of polarity has indeed been recorded in observational data in the coastal ocean for long nonlinear waves where a change of sign in the nonlinear coefficient of the underlying Korteweg-de Vries equation is indicative of a polarity reversal [2,3].

The long-short wave resonance system for a complex-valued short wave envelope S and a real-valued long wave L, obtained through a multiple scale expansion setting is given by [8]

$$iS_t + \lambda_1 S_{xx} = \gamma_1 LS, \quad L_t = \mu_1(|S|^2)_x. \tag{1}$$

The parameters λ_1, γ_1, and μ_1, measure the effects of dispersion, nonlinear coupling, and radiation stress of the short waves acting on the long wave, respectively. The precise numerical values of these parameters will depend on the physical context, which here is a density stratified fluid. The dispersion of the short wave envelope is balanced by the nonlinear interaction with the long wave. In contrast, the mean flow (long wave) of a weakly nonlinear, narrow-band packet is generated by self-interaction of the short wave through the radiation stress term [8]. Asymptotically, the group velocity coordinate of "long-short" resonance is associated with $\varepsilon^{2/3}x$ and $\varepsilon^{2/3}t$, where ε is a nondimensional, small amplitude parameter. The evolution time scale for the long-short system is $\varepsilon^{4/3}t$, rather than the $\varepsilon^2 t$ of the nonlinear Schrödinger equation model. The mean flow of the long-short resonance system is of order $\varepsilon^{4/3}$.

A remark on the physical origin of Eq. (1) is in order. While linear theory will predict particle paths to be strictly periodic orbits (circular or elliptical), nonlinear effects will displace the fluid

downstream in the propagation direction, resulting in the well-known "Stokes drift", which is proportional to the square of the wave amplitude. Further, when a wave packet is considered, that is the wave amplitude is spatially modulated, a radiation stress is formed which generates a wave-induced mean flow also proportional to the square of the wave amplitude. This interacts with the primary harmonic, and together with the interaction of the primary harmonic with the induced second harmonic, and cubic interactions of the primary harmonic, lead to the cubic nonlinear term in the widely studied nonlinear Schrödinger model.

On the other hand, a triad resonance arises for a special combination of linear waves where spontaneous generation of one member is possible due to special wave numbers and frequencies dictated by the dispersion relation. Long-short wave resonance is a special case of triad resonance where two members are nearly identical while a third one is much longer. Indeed this third member effectively serves as the "mean flow" [L of Eq. (1)] of the system, whereas the "mean flow" of the nonlinear Schrödinger equation model is the slaved amplitude-dependent wave-induced mean flow. This provides a physical explanation for the first component of Eq. (1). The second component can be interpreted as the slow evolution of the long wave component being modulated by the interaction of two nearly identical short waves, expressed as a radiation stress term.

The governing equations, boundary conditions and precise scaling will be described in Secs. II and III. Weakly nonlinear theory has an intrinsic assumption of a small amplitude parameter. Truly large amplitude and fully nonlinear waves must be investigated by numerical simulations or higher-order perturbation series. Nevertheless, weakly nonlinear models serve as a preliminary analysis in providing useful insights. Moreover, the rogue waves of lowest order in the $(2+1)$-dimensional long wave-short wave resonance system are long crested, which justified the $(1+1)$-dimensional approach [21]. Investigation on higher order rogue waves with more complex structures in the $(2+1)$-dimensional system will be carried out in subsequent works.

Without loss of generality, system (1) can be normalized through a scaling

$$iS_\tau - S_{xx} = \tilde{L}S, \quad \tilde{L}_\tau = -\sigma(|S|^2)_x, \tag{2}$$

$$\tau = -\lambda_1 t, \quad \tilde{L} = -\frac{\gamma_1}{\lambda_1}L, \quad \sigma = -\frac{\gamma_1\mu_1}{\lambda_1^2}. \tag{3}$$

The explicit form of a rogue wave as an exact breather solution of Eq. (2) is given in our earlier work [19], and is also reproduced in Appendix A for completeness. An important goal here is to study how the properties of this rogue wave will be affected by the specific fluid configuration. In contrast to the well-known Peregrine breather of the nonlinear Schrödinger equation, rogue wave modes always exist for Eq. (2) regardless of the sign of the parameter σ. For this normalized system, both the short wave and long wave are elevation (or "bright", borrowing a term from optics) rogue waves [19]. For the short wave S, the amplification ratio of the rogue wave from the background amplitude is two. The maximum of the internal long wave mode is attained at $(x,\tau) = (0,0)$ with

$$\tilde{L}(0,0) = 3\left(2\sigma s_0^2\right)^{2/3}, \tag{4}$$

where s_0 is the background amplitude of the short wave component and is taken as one in the following analysis. The rogue wave profiles in the fluid domain are then recovered through the rescaling in Eq. (3). We shall refer to this extremum of L as the normalized amplitude of the rogue wave for the long wave component. Remarkably, the polarity of the rogue wave would change if the nonlinearity γ_1 changes sign. This change is reminiscent of a similar transformation for a soliton in the long wave regime, where the quadratic nonlinearity in the Korteweg-de Vries equation changes sign [22].

In practice, there may be a small deviation from the exact resonance condition. To account for such deviation in wave number (κ) of the carrier wave train, a correction of the form $\exp[i(\kappa x - \Omega t)]$ is incorporated in S. Mathematically, this is equivalent to considering a *detuned*

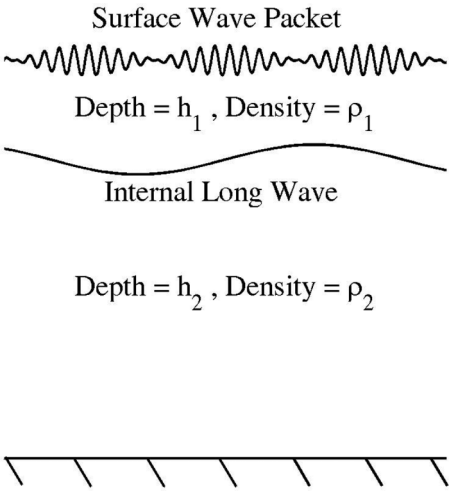

FIG. 1. The two-layer fluid model in the physical domain. In nondimensional units, the depth of the upper layer is the characteristic length.

system [19],

$$i\tilde{S}_\tau - 2i\kappa\tilde{S}_x - \tilde{S}_{xx} = \tilde{L}\tilde{S}, \quad \tilde{L}_\tau = -\sigma(|\tilde{S}|^2)_x. \tag{5}$$

The resulting rogue wave mode of Eq. (5) can be an elevation (bright), a depression (dark) or a four-petal shaped unit with two peaks and two depressions [20]. This contrasts strongly with the case with $\kappa = 0$ (corresponding to exact resonance), where the rogue wave must be an elevation. In this work, we focus on the case of exact resonance ($\kappa = 0$).

The remaining structure of this paper is as follows. First in Sec. II we consider a two-layered fluid model. In general, the rogue wave mode displays no peculiarities, that is, the polarity of the rogue wave is not dramatically affected by the depth and density ratios. In Sec. III we consider the case of a constant buoyancy frequency, which permits a complete theoretical analysis, and in Sec. IV we use a hyperbolic secant profile in the buoyancy frequency. These cases are more intriguing. The role of modulation instability on the generation of these rogue waves is discussed in Sec. V.

II. TWO-LAYER FLUID MODEL

A two-layer fluid model of piecewise homogeneous fluids offers a simplified approach. Although a Hamiltonian formulation for flows with constant vorticity in each layer is possible [23], only the irrotational case is considered here. The jump conditions for the continuity of vertical displacement and pressure at each interface then complete the formulation. For special values of the wave number, resonance can occur between a surface wave and an interfacial wave. This allows us to examine the effects of the density stratification and the depth ratio between the two layers on the structure of the rogue waves.

More precisely, in the undisturbed state we consider a homogeneous fluid of density ρ_2 and depth h_2 located below another homogeneous fluid of density $\rho_1 = \rho_2(1 - \Delta)$ and depth h_1 (Fig. 1). We consider a nondimensional system where acceleration due to gravity is unity and set $y = 0$ as the undisturbed interface between the two layers. Velocity potentials in the upper (lower) layer $\tilde{\phi}_1(\tilde{\phi}_2)$ satisfy the Laplace equation due to mass conservation for irrotational flows [8],

$$\tilde{\phi}_{1xx} + \tilde{\phi}_{1yy} = 0, \ \zeta < y < h_1 + \xi; \quad \tilde{\phi}_{2xx} + \tilde{\phi}_{2yy} = 0, \ -h_2 < y < \zeta,$$

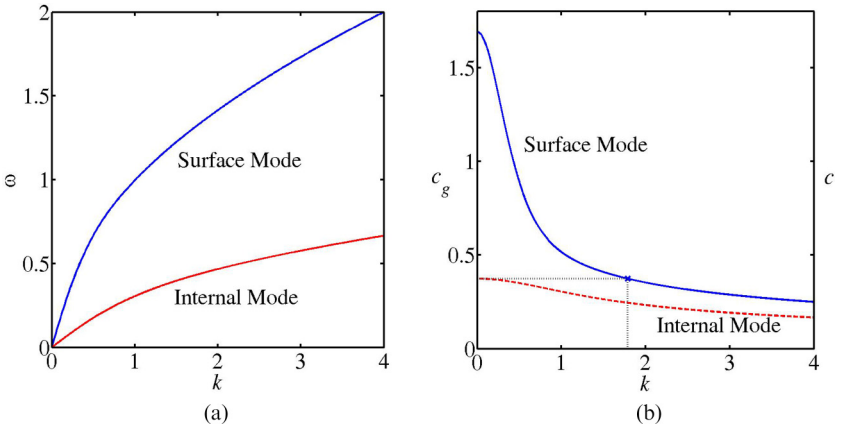

FIG. 2. (a) Dispersion relation of the two-layer model; (b) group velocity (c_g) of the surface mode (solid line) and the phase velocity (c) of the internal mode (dashed line). Resonance occurs at $k = 1.79$ for this case with $\Delta = 0.2$ and $h = 2$.

where ζ and ξ are the interfacial and surface displacements. The kinematic boundary condition is applied at the interface and the free surface:

$$\xi_t + \tilde{\phi}_{1x}\xi_x = \tilde{\phi}_{1y} \quad \text{at } y = h_1 + \xi,$$

$$\zeta_t + \tilde{\phi}_{1x}\zeta_x = \tilde{\phi}_{1y},\ \zeta_t + \tilde{\phi}_{2x}\zeta_x = \tilde{\phi}_{2y}, \quad \text{at } y = \zeta.$$

The dynamic boundary conditions require that the pressure be (a) continuous across the interface and (b) constant at the free surface. Using the Bernoulli equation, these requirements give

$$\tilde{\phi}_{1t} + \xi + \tfrac{1}{2}\left(\tilde{\phi}_{1x}^2 + \tilde{\phi}_{1y}^2\right) = 0, \quad \text{at } y = h_1 + \xi,$$

$$(1-\Delta)\left[\tilde{\phi}_{1t} + \zeta + \tfrac{1}{2}\left(\tilde{\phi}_{1x}^2 + \tilde{\phi}_{1y}^2\right)\right] = \left[\tilde{\phi}_{2t} + \zeta + \tfrac{1}{2}\left(\tilde{\phi}_{2x}^2 + \tilde{\phi}_{2y}^2\right)\right], \quad \text{at } y = \zeta.$$

Furthermore, rigid boundary condition is imposed at the bottom $y = -h_2$. To simplify the discussions, we adopt further nondimensional scaling where the fluid depth of the upper layer, wave speed for the surface long wave and the density of the bottom layer are the characteristic scales for length, velocity, and density, respectively [8]. The dispersion relation for linear (small amplitude) sinusoidal waves of angular frequency ω and wave number k is then [Fig. 2(a)]

$$\omega^4[1 + (1-\Delta)\eta_1\eta_2] - \omega^2 k(\eta_1 + \eta_2) + \Delta k^2 \eta_1\eta_2 = 0, \tag{6a}$$

$$\text{where } \eta_1 = \tanh(k), \quad \eta_2 = \tanh(kh), \text{ and } h = h_2/h_1. \tag{6b}$$

The small parameter ε used in the asymptotic expansion will be the ratio of the free surface or interfacial displacement to fluid depths, i.e., $\varepsilon \ll 1$, $h = O(1)$. We shall examine values of ε in the range 0.02–0.05, and use a density difference Δ in the range 0.2–0.5. Hence it is permissible to use the same reference scale for surface and interfacial displacements.

The two frequencies (ω) correspond to the surface mode and the internal mode. Long-short wave resonance occurs if the linear phase velocity c of the (long) internal wave ($k \to 0$),

$$c^2 = \frac{1 + h - \sqrt{(1+h)^2 - 4\Delta h}}{2}, \tag{7}$$

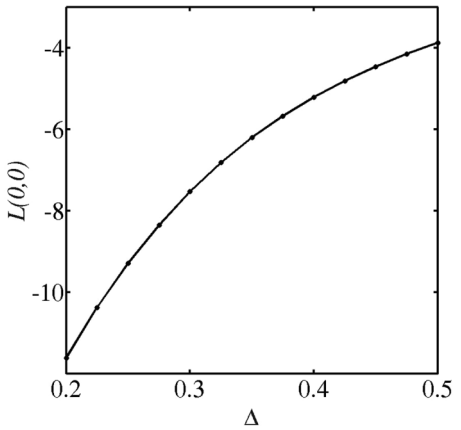

FIG. 3. Effect of density difference on the normalized amplitude of the internal rogue wave at $h = 2$.

matches the linear group velocity c_g of the (short) surface wave packet,

$$c_g = \frac{d\omega}{dk}, \quad \text{where } \omega^2 = \frac{k\left\{\eta_1 + \eta_2 + \sqrt{(\eta_1+\eta_2)^2 - 4\Delta\eta_1\eta_2[1+(1-\Delta)\eta_1\eta_2]}\right\}}{2[1+(1-\Delta)\eta_1\eta_2]}. \tag{8}$$

This equality determines the wave number for a resonance as a function of h and Δ [Fig. 2(b)]. The coefficients in the long wave-short wave system (1) can be found in the literature and are presented in Appendix B [8].

Since the scaling in Eq. (3) does not affect the sign of the short wave component, the short wave envelope is still an elevation rogue wave upon scaling the rogue wave solution given in Appendix A [19]. In the following, we focus on the polarity of the long wave component. Remarkably, this component is usually a depression rogue wave, independent of the depth ratio and density difference. The words "elevation" and "depression" are used to describe the main displacement of the rogue wave. While the fast oscillations inside the carrier envelope might go above and below the average position regularly, the envelope itself is represented by an algebraic expression depicting elevation (depression) above (or below) the background plane wave respectively.

A. Effect of density stratification

To study the effect of the density difference, the extremum of L is computed for various values of Δ (Fig. 3, for $h = 2$). The long wave mode is then a depression mode with the main displacement below the mean level. As the difference between the densities decreases, the restoring force due to buoyancy becomes smaller and the depression rogue wave can attain a larger amplitude. Similar results can be obtained for other values of the depth ratio. For application to realistic ocean situations, the density difference is small and Δ may typically take values around 0.01 or even smaller. The frequency of the internal mode is then small, and resonance would occur only at large values of the wave number for the short wave. For example, for $\Delta = 0.01$ and $h = 2$, the resonance condition is fulfilled at $k = 37.4$. For such small density difference, the amplitude of the corresponding internal solitons or rogue waves could be exceedingly large. As this scenario may compromise the asymptotic scaling and ordering of the perturbation sequence, a more detailed study will be pursued in the future.

B. Effect of depth ratio

The influence of the depth ratio between the two layers is less drastic when compared with the effect of the density difference. The internal mode is always a depression rogue wave even when

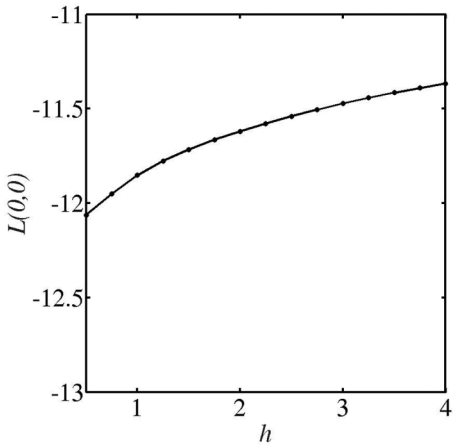

FIG. 4. Effect of depth ratio on the normalized amplitude of the internal rogue wave at $\Delta = 0.2$.

the upper layer is deeper ($h = 0.5$ in Fig. 4). This contrasts sharply with the classical nonlinear long wave theory based on equations of the Korteweg-de Vries type, where the interfacial solitary bulges towards the fluid of greater depth [24].

III. MODEL WITH CONSTANT BUOYANCY FREQUENCY

The two-layer fluid is a coarse approximation, as the density variation in a real oceanic pycnocline may be rapid but is nevertheless continuous. As a different approach we consider a uniformly and continuously stratified fluid confined between rigid boundaries at $y = y_1$ and $y = y_2$ with a typical buoyancy frequency of N_{ref}. The Boussinesq approximation is invoked. With length, time, velocity being nondimensionalized respectively by h_3 (channel depth), N_{ref}, and $N_{\text{ref}} h_3$, a nonlinear evolution equation can be established for the stream function [10]. A small parameter is taken as the ratio of wave amplitude to h_3. Asymptotic expansion of a slowly varying wave packet can be performed for the regime of long-short wave resonance, and the nondimensional governing system then takes the form,

$$i S_t + \lambda_2 S_{xx} = \gamma_2 L S, \quad L_t = \mu_2 (|S|^2)_x, \tag{9}$$

where the coefficients are reproduced in Appendix C [10]. We study elevation or depression rogue waves for a fluid with a constant buoyancy frequency:

$$N(y) = N_0. \tag{10}$$

The channel is taken as $y_1 = -1$ and $y_2 = 1$. It is possible to normalize N_0 through rescaling time. However, in order to study the effect of density variation, the reference buoyancy frequency N_{ref} is fixed and the nondimensional buoyancy frequency N_0 is varied.

As an illustrative example, only *odd* linear modes will be considered and it is sufficient to take the domain as the interval [0, 1]. The linear vertical velocity of the nth mode (n positive integer) is given by Eq. (C1) as [25]

$$\phi = \sin(by), \quad b = n\pi. \tag{11}$$

The rigid boundary conditions at the wall give the dispersion relation [Fig. 5(a)]

$$\omega^2 = \frac{N_0^2 k^2}{n^2 \pi^2 + k^2}. \tag{12}$$

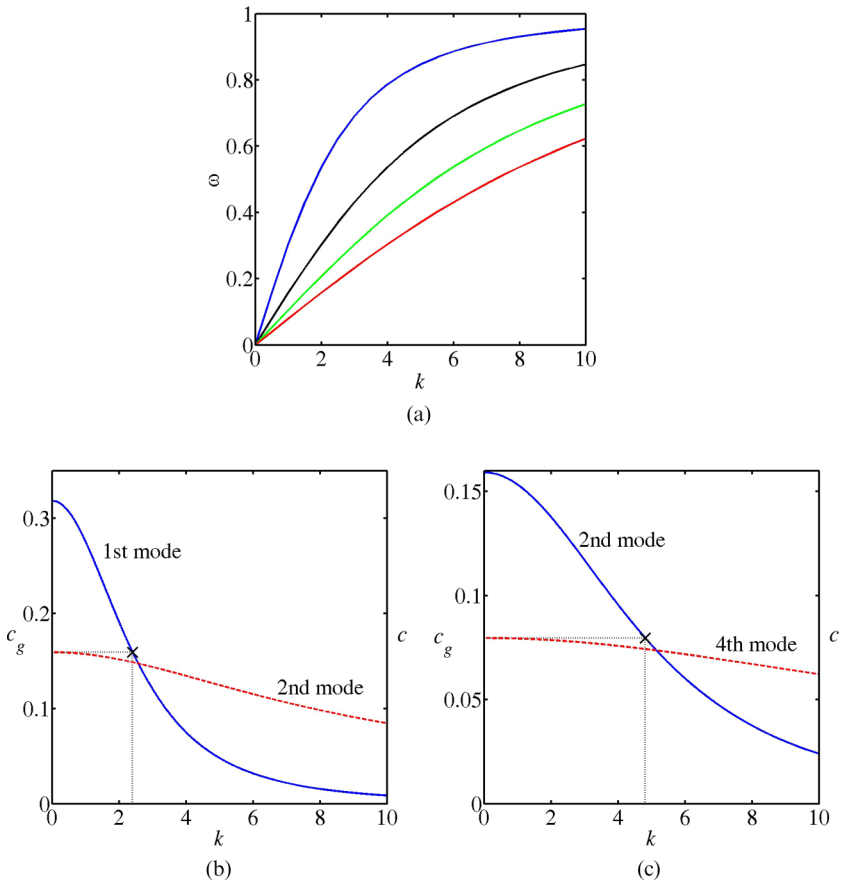

FIG. 5. (a) Dispersion curves of the first four modes for $N_0 = 1$. (b) Group velocity (c_g) of the first mode (solid line) and the phase velocity (c) of the second mode (dashed line). Resonance occurs between the first and second mode at the wave number marked by a cross. (c) Group velocity (c_g) of the second mode (solid line) and the phase velocity (c) of the fourth mode (dashed line). Resonance occurs between the second and fourth mode at the wave number marked by a cross.

Unlike the two-layer model of Sec. II, a continuously stratified fluid permits an infinite number of modes. Long-short wave resonance can thus arise between various modes at different wave numbers. More precisely, resonance may occur between a short wave of the nth mode with wave number k and a long wave of the mth mode if k (of the nth mode) satisfies the relation [Fig. 5(b)]

$$k^2 = (m^{2/3}n^{4/3} - n^2)\pi^2, \tag{13}$$

and the corresponding group velocity is given by

$$c_g = \frac{N_0}{m\pi}. \tag{14}$$

With this special value of group velocity, the "mean flow" [Eq. (C2)] is thus

$$\Phi = \sin(m\pi y). \tag{15}$$

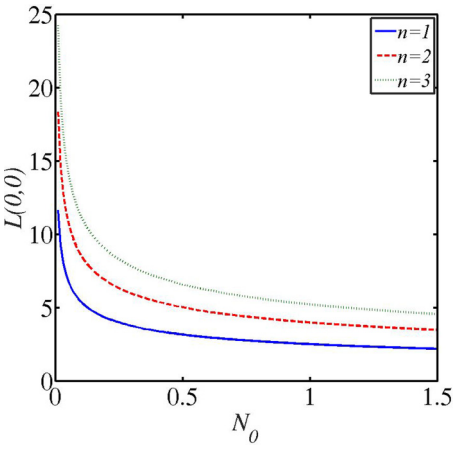

FIG. 6. The effect of buoyancy frequency on the normalized amplitude of the internal rogue wave. As the buoyancy frequency decreases, the amplitude increases. For resonance between modes of higher mode numbers, the amplitude of the rogue wave increases: $n = 1$ (lower solid line); $n = 2$ (middle dashed line); $n = 3$ (upper dotted line).

The coefficients of nonlinear coupling (γ_2) and self-interaction (μ_2) will generally vanish. We focus on the exceptional case $m = 2n$ [Eqs. (13) and (C4)–(C6)]:

$$k_c^2 = k_0^2 n^2 \pi^2 \quad \text{where} \quad k_0^2 = 4^{\frac{1}{3}} - 1, \tag{16}$$

$$\lambda_2 = -\frac{3k_0}{2\pi^2\left(1+k_0^2\right)^{\frac{5}{2}}}\frac{N_0}{n^2} \approx -0.04\frac{N_0}{n^2}, \tag{17}$$

$$\gamma_2 = \frac{\pi^2 k_0^3\left(k_0^2+3\right)}{2}n^2 \approx 7.97n^2, \tag{18}$$

$$\mu_2 = -\frac{\pi k_0^2\left(k_0^2+3\right)}{8\left(k_0^2+1\right)^3}n \approx -0.21n. \tag{19}$$

Hence, the normalized amplitude of the internal rogue wave is given by

$$L(0,0) = \frac{9^{\frac{1}{3}}\left(k_0^2+3\right)^{\frac{1}{3}}\pi^{\frac{2}{3}}}{4^{\frac{1}{3}}\left(k_0^2+1\right)^{\frac{7}{6}}}\frac{n^{\frac{2}{3}}}{N_0^{\frac{1}{3}}} \approx 2.51\frac{n^{\frac{2}{3}}}{N_0^{\frac{1}{3}}}. \tag{20}$$

(1) *Elevation rogue wave:* For convenience a rogue wave mode is termed an elevation rogue wave if $L(0,\ 0)$ is positive. The actual physical quantities (displacement and velocities) will be the product $\Phi(y)L(x,t)$ or its derivative, and thus may oscillate with the vertical coordinate through $\Phi(y)$. Using such terminology, the long wave is always an elevation rogue mode [Eq. (20)]. The significance of this critical wave number k_c [Eq. (16)] is twofold. Not only it highlights the onset of long-short wave resonance, it also separates the focusing regime from the defocusing one for the nonlinear Schrödinger equation for a "narrow band" wave packet [25].

(2) *Effect of buoyancy frequency:* The amplitude $L(0,\ 0)$ will become larger with a smaller buoyancy frequency, as the reduced density variation gives rise to a taller rogue wave [Eq. (20) and Fig. 6].

(3) *Effect of mode number:* The order of the participating modes is also critical. For a fixed N_0, long-short wave resonance involving higher mode number (n) will yield rogue waves of a bigger

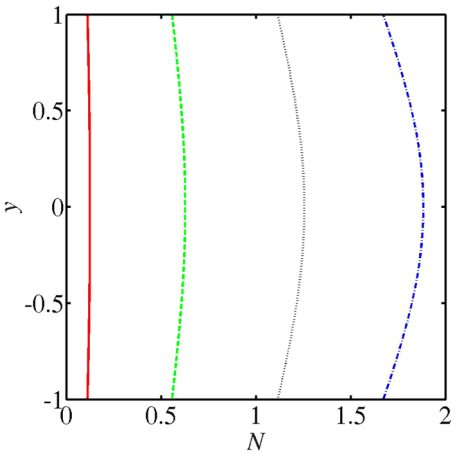

FIG. 7. Typical buoyancy frequency profiles for various input parameters: $\alpha = 0.1$ and $\beta = 0.00577$ (solid line); $\alpha = 0.5$ and $\beta = 0.144$ (dashed line); $\alpha = 1$ and $\beta = 0.577$ (dotted line); $\alpha = 1.5$ and $\beta = 1.297$ (dashed-dotted line), with $r = 0.659$ in all cases.

amplitude [Eq. (20) and Fig. 6]. This theoretical trend cannot continue indefinitely with larger n, as physically the larger values of wave number k [Eq. (16)], or exceedingly short waves, may render the asymptotic balance for the long-short scaling questionable.

IV. STRATIFIED FLUID MODEL WITH HYPERBOLIC SECANT BUOYANCY FREQUENCY

To further improve the modeling of the density stratification, a hyperbolic secant profile for the buoyancy frequency is considered. A local maximum in the buoyancy frequency corresponds physically to a greater change in the density profile. More precisely, a stratified fluid of buoyancy frequency

$$N^2 = \alpha^2 \mathrm{sech}^2(ry) + \beta, \tag{21}$$

with r, α and β being positive constants (Fig. 7), is located in a channel from $y_1 = -1$ to $y_2 = 1$. To obtain the dispersion relation for linear modes, the eigenvalue problem for the angular frequency ω for a given wave number k

$$-\frac{d^2\phi}{dy^2} + k^2\phi = \frac{1}{\omega^2} k^2 N^2 \phi \tag{22}$$

is solved with boundary conditions $\phi(-1) = \phi(1) = 0$. Remarkably, an exact solution of Eq. (C1) can be obtained at one specific value of the wave number k:

$$\phi = \mathrm{sech}^2(ry) - \frac{2}{3}. \tag{23}$$

Our strategy is to employ such special exact solutions to facilitate higher order calculations of the long-short wave resonance model, assisted by numerical solutions whenever necessary. Straightforward calculations now yield

$$r = \mathrm{sech}^{-1}\left(\sqrt{\frac{2}{3}}\right), \tag{24}$$

$$k = \frac{r\sqrt{6\beta}}{\alpha} \quad \text{and} \quad \omega = \sqrt{\beta}. \tag{25}$$

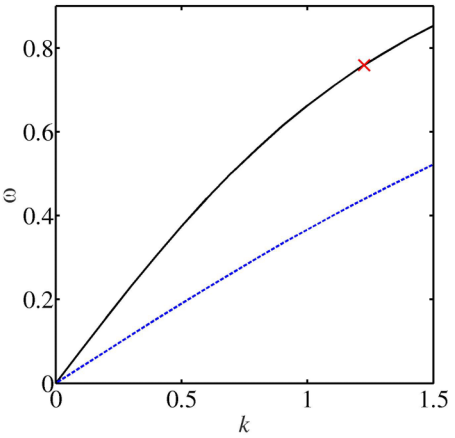

FIG. 8. Dispersion curves of the first two modes at $\alpha = 1$ and $\beta = 0.577$. The "cross" marks the wave number of the "short" first mode which is in resonance with the a long wavelength second mode.

A. Dispersion relation

For arbitrary wave number k, Eq. (22) is a Sturm-Liouville problem, and the Rayleigh-Ritz method can be applied to estimate the eigenvalues. Polynomials are employed here as trial functions:

$$w_j(y) = y^{j-1}(y^2 - 1), \quad \text{for } j = 1, \ldots, M. \tag{26}$$

To obtain the first few eigenvalues, polynomials of degree 12 are sufficient (i.e., $M = 11$). The dispersion curves of the first two linear modes of the stratification profile Eq. (21) can then be obtained (Fig. 8 using $\alpha = 1$, $\beta = 0.577$). Quality assurance checks are performed by increasing values of M, and also by employing a different basis set in the Rayleigh-Ritz procedure, e.g., hyperbolic functions. The results are in good agreement.

From the dispersion curves, the phase velocity of long wave mode at a small wave number can be estimated numerically. The short wave mode participating in the resonance can then be identified. As example, the phase velocity of a long wavelength second mode matches the group velocity of a special first mode given in Eq. (25) for $\alpha = 1$ and $\beta = 0.577$.

B. Formulation

The general formulation of the long-short wave resonance model for a continuously stratified fluid is given in Sec. III and Appendix C. Since the dispersion relation is obtained numerically, Eq. (C4) is utilized to compute the group velocity dispersion. Equation (C1) is differentiated with respect to k to yield an equation in ϕ_k,

$$\phi_{kyy} + k^2\left(\frac{N^2}{\omega^2} - 1\right)\phi_k = \left[2k\left(1 - \frac{N^2}{\omega^2}\right) + \frac{2N^2k^2\omega_k}{\omega^3}\right]\phi. \tag{27}$$

By reduction of order, the complementary functions of Eq. (27) are given by

$$\begin{aligned}
\theta_1(y) &= \operatorname{sech}^2(ry) - \frac{2}{3}, \\
\theta_2(y) &= \left[\operatorname{sech}^2(ry) - \frac{2}{3}\right]\int\left[\operatorname{sech}^2(ry) - \frac{2}{3}\right]^{-2} dy \\
&= \left[\operatorname{sech}^2(ry) - \frac{2}{3}\right]\left\{\frac{9y}{4} - \frac{27[2\exp(2ry) - 1]}{4r[\exp(4ry) - 4\exp(2ry) + 1]}\right\}.
\end{aligned} \tag{28}$$

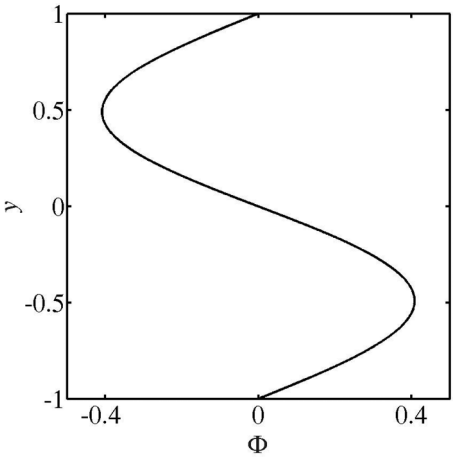

FIG. 9. Mean flow for a density stratification profile given by a hyperbolic function, Eqs. (21), (24), and (25): $\alpha = 1$, $\beta = 0.577$, and $k = 1.225$.

The particular solution can be obtained by variation of parameters. The group velocity dispersion can then be computed.

Secondly, the mean flow Φ can be found in terms of hypergeometric functions (Fig. 9). For the cases considered here, the odd solutions satisfy the boundary conditions:

$$\Phi(y) = -2\cosh^{G_2}(ry)\sinh(ry)F\left[\frac{1}{2}+\frac{G_2}{2}+i\sqrt{G_1},\frac{1}{2}+\frac{G_2}{2}-i\sqrt{G_1},\frac{3}{2},-\sinh^2(ry)\right],$$

where

$$G_1 = \frac{3\beta}{2\alpha^2}\left[\frac{\int_{-1}^{1}N^2\phi^2dy}{\int_{-1}^{1}(N^2-\beta)\phi^2dy}\right]^2, \quad G_2 = \frac{1}{2}\left\{1+\sqrt{1+24\left[\frac{\int_{-1}^{1}N^2\phi^2dy}{\int_{-1}^{1}(N^2-\beta)\phi^2dy}\right]^2}\right\},$$

and F is the hypergeometric function [26].

C. Results

To examine the effect of density variation, the maximum displacements at various values of α are computed (Table I). In all cases here, the resonance occurs between short wave of the first mode and long wave of the second mode. The long wave component is an elevation rogue wave, which gets taller as the average N^2 gets smaller (Fig. 7), a trend readily explained by the notion of buoyancy. Furthermore, with a smaller spatial variation in the buoyancy frequency (smaller α, Table I), the rogue wave gets taller too. However, modes fulfilling the resonance condition do not automatically

TABLE I. Effect of density variation on the normalized amplitude of the rogue wave.

α	β	k	$L(0,0)$
0.1	0.00577	1.225	4.268
0.5	0.144	1.225	2.496
1	0.577	1.225	1.981
1.5	1.297	1.225	1.731

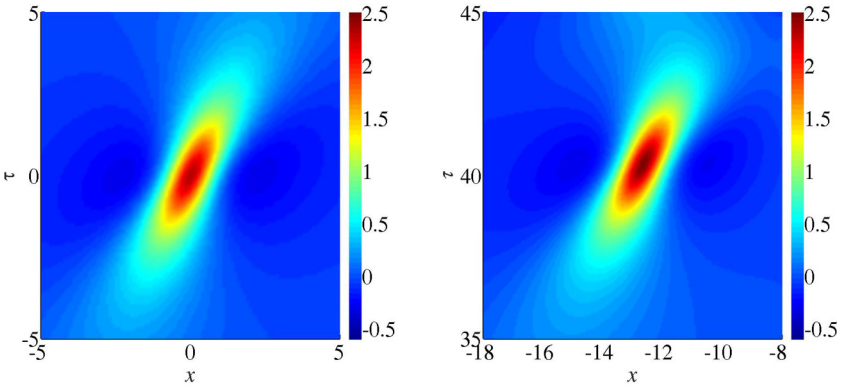

FIG. 10. Generation of rogue wave from baseband modulation instability: (a) analytical rogue wave solution for $\sigma = 1.36$ and $s_0 = 0.5$; (b) rogue wave mode generated from a wavy disturbance with small wave number ($K = 0.2$) and 0.1% amplitude.

imply generation of rogue waves, as the resulting nonlinear coefficients may vanish, and hence the elaborate analysis presented here is valuable.

V. ROGUE WAVES GENERATED FROM BASEBAND DISTURBANCES

While rogue wave modes have been analytically derived for many dynamical systems, their generation from arbitrary initial conditions still remains an issue of intense debate. One school maintains that "baseband instability" (long wavelength regime of modulation instability) will be essential for the occurrence of rogue waves [27]. At the other end of the spectrum of diverse opinions, there are suggestions that modulation instability will not play a key role in the dynamics [28].

The connection between the onset of baseband instability and the existence condition of rogue waves has been established analytically for many nonlinear evolution systems [29]. This generation mechanism can be further substantiated by choosing one special baseband mode as the initial condition [30]. By perturbing the background short wave envelope (long wave) with $\exp(iKx)$ [$\cos(Kx)$], respectively, that is,

$$S(x,0) = [1 + 0.001 \exp(iKx)]\, s_0, \quad \tilde{L}(x,0) = 0.001 \cos(Kx), \tag{29}$$

localized entities [Fig. 10(b)] resembling the rogue waves can be generated [Fig. 10(a)].

To further elucidate this idea in a physically realistic setting, chaotic wave fields are generated by a random noise containing modes of various wave numbers. The initial condition is given by

$$S(x,0) = \{1 + 0.001[1 - 2\nu(x)]\} s_0, \quad \tilde{L}(x,0) = 0.001[1 - 2\nu(x)], \tag{30}$$

where $\nu(x)$ is a random function uniformly distributed in the interval (0,1) and hence the spectrum will cover a wide range of frequencies. Rogue wave modes exist in a chaotic wave field provided that baseband modes are unstable [27]. Among various breather-like entities in the chaotic field [Fig. 11(a)], localized modes with waveform similar to a rogue wave can be observed [Fig. 11(b)]. We can thus assert that baseband instability plays a crucial role in the generation of rogue waves.

VI. DISCUSSIONS AND CONCLUSIONS

While rogue waves on the sea surface have recently been intensively studied theoretically and experimentally, our aim here is to examine analytically if such unexpectedly large amplitude waves

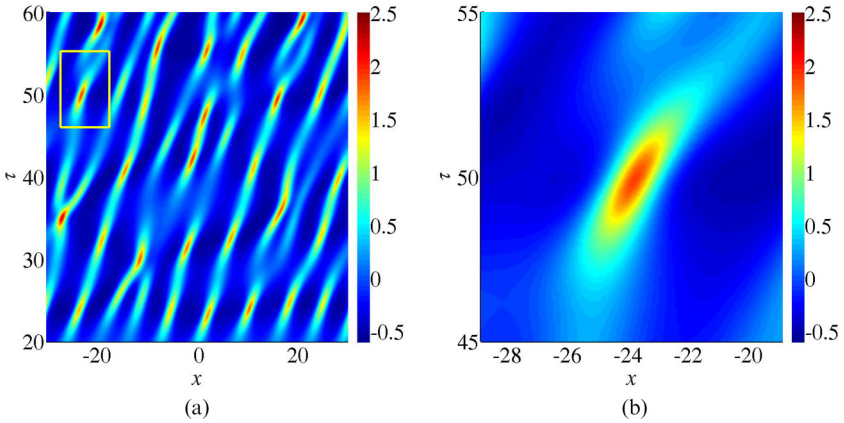

FIG. 11. (a) Observation of rogue wave modes in a chaotic wave field ($\sigma = 1.36$ and $s_0 = 0.5$); (b) an enlarged view of the localized peak enclosed by a square frame as indicated in panel (a).

can also occur as internal waves, using the long-short wave resonance as an illustrative example. The analysis confirms the existence of such waves and also highlights that the nonlinear dynamics can be quite different from that of the well-known nonlinear Schrödinger equation. For this internal wave setting, the timescale of evolution is faster asymptotically ($\varepsilon^{4/3}t$ versus $\varepsilon^2 t$ of the Schrödinger model, ε being a nondimensional small amplitude parameter). Furthermore, the amplification ratio is not restricted to three times the background plane wave (the case for the nonlinear Schrödinger equation), and there is no constraint on the signs of the nonlinearity and dispersion. Moreover, the nonlinear Schrödinger model imposes a restriction of $kH > 1.363$ for modulation instability of water waves (and so for rogue waves) where k is the wave number of the carrier waves, and H is the water depth. However, there are no such corresponding requirements for this long-short wave resonance.

An important result is that the character of these "internal" rogue waves will depend critically on the stratification profile and the precise nature of the internal modes involved. As illustrative examples, three density profiles were considered. First, a two-layer fluid model with a jump in density at the interface was investigated. Second, to provide a better model for a smooth transition at the pycnocline, two models with continuous density stratification were considered, a case with constant buoyancy frequency and a case with buoyancy frequency taking up a hyperbolic secant profile. One major difference between the two-layer model and the continuously stratified models is that the latter allow infinitely many modes. As a result, long-short wave resonance may occur between various pairs of modes. These density profiles have all been commonly used in the literature. We note in particular the study of Stokes drift for internal equatorial Kelvin waves, where both continuously stratified and two-layer models had been employed [31]. Indeed the two-layer model for internal waves had been extended to the case where each layer itself consisted of fluid with constant buoyancy frequency [32].

Further, the effect of density variations on the amplitude of the rogue waves was examined. In general, a smaller jump in density would give rise to a rogue wave with a larger amplitude, as the effect of buoyancy will be reduced. For an elevation or depression rogue wave, the maximum height or depth attained is larger when the density difference is reduced respectively. This is true for both layered and continuously stratified models, independent of whether the change in density is gradual or abrupt. On the other hand, the change in depth ratio causes only minor effect on the amplitude of the rogue wave.

For continuously stratified fluids, there may be an infinite number of linear modes. However, generation of rogue waves is not automatic or spontaneous, as the nonlinear dynamics depends critically on the nature of the participating modes. Although the resonance condition can be fulfilled,

the evolution systems may have zero coefficients, and the dynamics is degenerate. For a stratified fluid with constant buoyancy frequency, the wave number of a special, first internal mode in resonance with a long, second internal mode will permit the occurrence of rogue waves. This critical wave number [Eq. (16)] also highlights the boundary of the focusing/defocusing regimes in the context of the nonlinear Schrödinger equation. Similar resonances involving other internal modes pairs (a short second order mode and a long fourth order mode) also exist. The amplitude of the rogue wave will depend on the participating modes.

To elucidate the importance of baseband modulation instability, rogue waves are generated numerically from initial conditions consisting solely of baseband modes. Similar rogue-wave-like structures are observed from a chaotic wave field too, but the amplitude and time of formation are slightly different.

All these and related issues remain to be resolved in the future. First, rigid wall conditions versus the presence of a free surface may influence the outcome. Second, resonant interactions in the presence of nonzero vorticity have not been considered here [33]. To give a better modeling of geophysical phenomena, such as the Equatorial Undercurrent [34], the effect of background current shear on internal rogue waves will be investigated in future works. Moreover, the complexity of the density configuration will be improved to include thermohaline staircases or multiple stratified fluid patches [35,36]. Thermohaline staircases are indeed observed in many places, including both warm regions and cold regions like the Arctic Ocean [35,37,38]. Hence, extensions of the present work to include multiple layers with piecewise constant or smooth density profiles would be valuable in applications to physical oceanography. We note that the present long-short wave resonance condition for the constant buoyancy frequency case coincides with that obtained in the literature in a different context [39], where the issues of momentum and impulse in stratified flows were treated. Another interesting aspect is the interaction of multiple wave trains [29]. The effect of density stratification on the evolution of rogue waves in coupled systems will also be considered in future efforts. The main information here is that the precise structure of the density stratification profiles will have a profound influence on the generation and nature of rogue waves in the interior of a fluid [40,41]. Finally, the present work imposes a localized flow structure in the vertical direction, and the stratified fluid forms a wave guide for wave propagation in the horizontal direction. In contrast, several other works in the literature allow wave propagation in the vertical direction as well [42,43]. Further theoretical works along these directions will definitely be fruitful.

ACKNOWLEDGMENTS

Partial financial support has been provided by the Research Grants Council through contracts HKU17200718E and HKU17200815. Computing facilities at the University of Hong Kong Information Technology Services are supported by the Hong Kong University Grants Committee Special Equipment Grant (SEG HKU09). R.H.J.G. was supported by the Leverhulme Trust through the award of a Leverhulme Emeritus Fellowship (EM-2015-37).

APPENDIX A

The rogue wave solution of the long-short system Eq. (2) is given by [19]

$$
\begin{aligned}
S &= s_0\left\{1+\frac{-4+4\Omega_i i x+4\left(\Omega_r^2-\Omega_i^2\right) i\tau}{\left(\Omega_r^2+\Omega_i^2\right)\left[(x-\Omega_i\tau)^2+\Omega_r^2\tau^2+1/\Omega_r^2\right]}\right\},\\
\tilde{L} &= \frac{4}{\left[(x-\Omega_i\tau)^2+\Omega_r^2\tau^2+1/\Omega_r^2\right]}-\frac{8(x-\Omega_i\tau)^2}{\left[(x-\Omega_i\tau)^2+\Omega_r^2\tau^2+1/\Omega_r^2\right]^2},\\
\Omega_r &= \frac{\sqrt{3}}{2}\sqrt[3]{2\sigma s_0^2},\ \ \Omega_i=\frac{1}{2}\sqrt[3]{2\sigma s_0^2},
\end{aligned}
\tag{A1}
$$

where s_0 is the background amplitude of the short wave component, and $\Omega_r + i\Omega_i$ is the leading order frequency in a long wave expansion of the dispersion relation with input from the density stratification profile. The long wave component usually does not change polarity [29]. Equation (A1) represents a pulse algebraically localized in both space and time.

APPENDIX B

The parameters in Eq. (1) for a two-layer fluid are given by [8]

$$\lambda_1 = \frac{1}{2}\frac{d^2\omega}{dk^2}, \quad \gamma_1 = \frac{\gamma_{11}}{\gamma_{12}}, \quad \gamma_{12} = \frac{2k(\eta_1+\eta_2)}{\omega^2} - 4[1+(1-\Delta)\eta_1\eta_2],$$

$$\begin{aligned}\gamma_{11} = \omega\Bigg(&k\Delta\left(1-\frac{k^2}{\omega^4}\right)(\eta_2-\eta_1) + \frac{2k\Delta}{\omega c_g}\left(\frac{k\eta_1}{\omega^2}-1\right)\\ &+ \frac{c_g}{c_g^2-1}\Bigg\{kc_g\left(1-\frac{k^2}{\omega^4}\right)\left[\eta_1+\eta_2-\Delta\eta_2\left(1+\frac{k\eta_1}{\omega^2}\right)\right]\\ &- \frac{2k(1-\Delta)(1+\eta_1\eta_2)}{\omega} - \frac{2\Delta k^2\eta_1}{\omega^3}\left(1-\frac{k\eta_2}{\omega^2}\right)\Bigg\}\Bigg),\end{aligned}$$

$$\begin{aligned}\mu_1 = \frac{h}{2\left[(1+h)c_g^2-2\Delta h\right]}\Bigg\{&(1-\Delta)c_g\left(\omega^2-\frac{k^2}{\omega^2}\right) - \frac{2(1-\Delta)kc_g^2}{\omega}\\ &- 2\omega c_g^2(1-\Delta)\left(\cosh k - \frac{k}{\omega^2}\sinh k\right)\left(\sinh k - \frac{k}{\omega^2}\cosh k\right)\\ &+ \left[\omega^2 c_g\left(1-c_g^2\right)\left(\frac{1}{\eta_2^2}-1\right) + \frac{2\omega\left(\Delta-c_g^2\right)}{\eta_2}\right]\left(\cosh k - \frac{k}{\omega^2}\sinh k\right)^2\Bigg\}.\end{aligned}$$

The above expressions are evaluated at k for which the resonance condition $c = c_g$ is satisfied.

APPENDIX C

For a continuously stratified fluid, the spatial structure of the vertical component of velocity, $\phi(y)$, is governed by the modal equation [10],

$$\frac{d^2\phi}{dy^2} + k^2\left(\frac{N^2}{\omega^2}-1\right)\phi = 0, \quad \text{in } y_1 < y < y_2, \tag{C1}$$

where N is the buoyancy frequency, k is the wave number, and ω is the angular frequency. Rigid wall conditions are imposed at the boundaries,

$$\phi(y_1) = \phi(y_2) = 0.$$

Using an asymptotic expansion of the form

$$\varepsilon\phi(y)[Se^{i(kx-\omega t)} + \text{c.c.}] + \varepsilon^{\frac{4}{3}}\Phi(y)L + \cdots,$$

the mean flow $\Phi(y)$ is obtained by solving the differential equation

$$\frac{d^2\Phi}{dy^2} + \frac{N^2}{c_g^2}\Phi = 0, \quad \text{in } y_1 < y < y_2, \tag{C2}$$

under the boundary conditions $\Phi(y_1) = \Phi(y_2) = 0$. The parameters in Eq. (9) are given by

$$c = \frac{\omega}{k}, \quad c_g = c\left[1 - \omega^2 \frac{\int_{y_1}^{y_2} \phi^2 dy}{\int_{y_1}^{y_2} N^2 \phi^2 dy}\right], \tag{C3}$$

$$\lambda_2 = \frac{1}{2}\frac{d^2\omega}{dk^2} = \frac{\omega}{2k^2}\left[-\frac{3c_g}{c}\left(1 - \frac{c_g}{c}\right) + 2k\left(1 - \frac{c_g}{c}\right)\frac{\int_{y_1}^{y_2} N^2 \phi\phi_k dy}{\int_{y_1}^{y_2} N^2 \phi^2 dy} - 2k\omega^2 \frac{\int_{y_1}^{y_2} \phi\phi_k dy}{\int_{y_1}^{y_2} N^2 \phi^2 dy}\right], \tag{C4}$$

$$\gamma_2 = -\frac{k(c/c_g)^2}{2\int_{y_1}^{y_2} N^2 \phi^2 dy} \int_{y_1}^{y_2} \left[\left(1 - \frac{c_g}{c}\right)\left(1 + \frac{2c_g}{c}\right) N^2 \phi^2 \Phi' + \left(1 + \frac{c_g}{c}\right)\phi^2 \Phi (N^2)'\right] dy, \tag{C5}$$

$$\mu_2 = -\frac{c_g/c}{2\int_{y_1}^{y_2} N^2 \Phi^2 dy} \int_{y_1}^{y_2} \left[\left(1 - \frac{c_g}{c}\right)\left(1 + \frac{2c_g}{c}\right) N^2 \Phi (\phi^2)' - \frac{2c_g}{c}\phi^2 \Phi (N^2)'\right] dy. \tag{C6}$$

[1] M. H. Alford, T. Peacock, J. A. MacKinnon *et al.*, The formation and fate of internal waves in the South China Sea, Nature (London) **521**, 65 (2015).

[2] K. R. Helfrich and W. K. Melville, Long nonlinear internal waves, Ann. Rev. Fluid Mech. **38**, 395 (2006).

[3] R. Grimshaw, E. Pelinovsky, T. Talipova, and A. Kurkina, Internal solitary waves: Propagation, deformation and disintegration, Nonlin. Proc. Geophys. **17**, 633 (2010).

[4] C. Garrett and W. Munk, Oceanic mixing by breaking internal waves, Deep-Sea Res. I **19**, 823 (1972).

[5] M. H. Alford, Redistribution of energy available for ocean mixing by long-range propagation of internal waves, Nature (London) **423**, 159 (2003).

[6] D. J. Benney, A general theory for interactions between short and long waves, Stud. Appl. Math. **56**, 81 (1977).

[7] A. D. D. Craik, *Wave Interactions and Fluid Flows* (Cambridge University Press, Cambridge, 1985).

[8] M. Oikawa, M. Okamura, and M. Funakoshi, Two-dimensional resonant interaction between long and short waves, J. Phys. Soc. Jpn. **58**, 4416 (1989).

[9] R. H. J. Grimshaw, The modulation of an internal gravity-wave packet, and the resonance with the mean motion, Stud. Appl. Math. **56**, 241 (1977).

[10] C. G. Koop and L. G. Redekopp, The interaction of long and short internal gravity waves: Theory and experiment, J. Fluid Mech. **111**, 367 (1981).

[11] C. Kharif, E. Pelinovsky, and A. Slunyaev, *Rogue Waves in the Ocean* (Springer, Berlin, 2009).

[12] K. Dysthe, H. E. Krogstad, and P. Müller, Oceanic rogue waves, Annu. Rev. Fluid Mech. **40**, 287 (2008).

[13] M. Onorato, S. Residori, U. Bortolozzo, A. Montina, and F. T. Arecchi, Rogue waves and their generating mechanisms in different physical contexts, Phys. Rep. **528**, 47 (2013).

[14] L. Shemer and L. Alperovich, Peregrine breather revisited, Phys. Fluids **25**, 051701 (2013).

[15] E. Pelinovsky, T. Talipova, and C. Kharif, Nonlinear dispersive mechanism of the freak wave formation in shallow water, Physica D **147**, 83 (2000).

[16] A. Chabchoub and M. Fink, Time-Reversal Generation of Rogue Waves, Phys. Rev. Lett. **112**, 124101 (2014).

[17] G. Ducrozet, M. Fink, and A. Chabchoub, Time-reversal of nonlinear waves: Applicability and limitations, Phys. Rev. Fluids **1**, 054302 (2016).

[18] A. Gill, *Atmosphere-Ocean Dynamics* (Academic Press, San Diego, 1982).

[19] K. W. Chow, H. N. Chan, D. J. Kedziora, and R. H. J. Grimshaw, Rogue wave modes for the long wave-short wave resonance model, J. Phys. Soc. Jpn. **82**, 074001 (2013).

[20] S. Chen, P. Grelu, and J. M. Soto-Crespo, Dark- and bright-rogue-wave solutions for media with long-wave-short-wave resonance, Phys. Rev. E **89**, 011201(R) (2014).

[21] J. Chen, Y. Chen, B. F. Feng, and K. Maruno, Rational solutions to two- and one-dimensional multicomponent Yajima-Oikawa systems, Phys. Lett. A **379**, 1510 (2015).
[22] R. Grimshaw, C. Wang, and L. Li, Modelling of polarity change in a nonlinear internal wave train in Laoshan Bay, J. Phys. Oceanogr. **46**, 965 (2016).
[23] A. Constantin, R. I. Ivanov, and C.-I. Martin, Hamiltonian formulation for wave-current interactions in stratified rotational flows, Arch. Rational Mech. Anal. **221**, 1417 (2016).
[24] T. Kakutani and N. Yamasaki, Solitary waves on a two-layer fluid, J. Phys. Soc. Jpn. **45**, 674 (1978).
[25] A. K. Liu and D. J. Benney, The evolution of nonlinear wave trains in stratified shear flows, Stud. Appl. Math. **64**, 247 (1981).
[26] M. Abramowitz and I. A. Stegun, *Handbook of Mathematical Functions* (Dover Publications, New York, 1964).
[27] F. Baronio, S. Chen, P. Grelu, S. Wabnitz, and M. Conforti, Baseband modulation instability as the origin of rogue waves, Phys. Rev. A **91**, 033804 (2015).
[28] F. Fedele, J. Brennen, S. P. de León, J. Dudley, and F. Dias, Real world ocean rogue waves explained without the modulational instability, Sci. Rep. **6**, 27715 (2016).
[29] H. N. Chan, E. Ding, D. J. Kedziora, R. Grimshaw, and K. W. Chow, Rogue waves for a long wave-short wave resonance model with multiple short waves, Nonlinear Dyn. **85**, 2827 (2016).
[30] H. N. Chan and K. W. Chow, Rogue waves for an alternative system of coupled Hirota equations: Structural robustness and modulation instabilities, Stud. Appl. Math. **139**, 78 (2017).
[31] J. E. H. Weber, K. H. Christensen, and G. Broström, Stokes drift in internal equatorial Kelvin waves: Continuous stratification versus two-layer models, J. Phys. Oceanogr. **44**, 591 (2014).
[32] A. Goullet and W. Choi, Large amplitude internal solitary waves in a two-layer system of piecewise linear stratification, Phys. Fluids **20**, 096601 (2008).
[33] C. I. Martin, Resonant interactions of capillary-gravity water waves, J. Math. Fluid Mech. **19**, 807 (2017).
[34] A. Constantin and R. S. Johnson, The dynamics of waves interacting with the Equatorial Undercurrent, Geophys. Astrophys. Fluid Dyn. **109**, 311 (2015).
[35] B. R. Sutherland, Internal wave transmission through a thermohaline staircase, Phys. Rev. Fluids **1**, 013701 (2016).
[36] B. R. Sutherland and K. Yewchuk, Internal wave tunnelling, J. Fluid Mech. **511**, 125 (2014).
[37] N. C. Shibley, M.-L. Timmermans, J. R. Carpenter, and J. M. Toole, Spatial variability of the Arctic Ocean's double-diffusive staircase, J. Geophys. Res. Oceans **122**, 980 (2017).
[38] Y. Bebieva and M.-L. Timmermans, The relationship between double-diffusive intrusions and staircases in the Arctic Ocean, J. Phys. Oceanogr. **47**, 867 (2017).
[39] M. E. McIntyre, Mean motions and impulse of a guided internal gravity wave packet, J. Fluid Mech. **60**, 801 (1973).
[40] R. Grimshaw, E. Pelinovsky, T. Talipova, and A. Sergeeva, Rogue internal waves in the ocean: Long wave model, Eur. Phys. J. Spec. Top. **185**, 195 (2010).
[41] T. G. Talipova, E. N. Pelinovsky, and Ch. Kharif, Modulation instability of long internal waves with moderate amplitudes in a stratified horizontally inhomogeneous ocean, JETP Lett. **94**, 182 (2011).
[42] B. R. Sutherland, Finite-amplitude internal wavepacket dispersion and breaking, J. Fluid Mech. **429**, 343 (2001).
[43] A. Tabaei and T. R. Akylas, Resonant long-short wave interactions in an unbounded rotating stratified fluid, Stud. Appl. Math. **119**, 271 (2007).